agriculture

MDPI

Article

Characterization of the Pore Network of a Cohesive Oxisol Through Morphological and Pore Complexity Analyses

Jocenei A. T. de Oliveira [1,*], Thaís N. Pessoa [2], José V. Gaspareto [1], Adolfo N. D. Posadas [3], André L. F. Lourenço [3], Paulo L. Libardi [2] and Luiz F. Pires [1]

[1] Laboratory of Physics Applied to Soils and Environmental Sciences, Department of Physics, State University of Ponta Grossa, Ponta Grossa CP 84030-900, Paraná, Brazil; 240304400000@uepg.br (J.V.G.); lfpires@uepg.br (L.F.P.)
[2] Department of Soil Science, "Luiz de Queiroz" College of Agriculture, University of São Paulo, São Paulo CP 13418-900, Sao Paulo, Brazil; thaisnpessoa@usp.br (T.N.P.); pllibard@usp.br (P.L.L.)
[3] AgriEntech Ltda., São Carlos CP 13560-460, São Paulo, Brazil; aposadas@agrientech.com (A.N.D.P.); alourenco@agrientech.com (A.L.F.L.)
* Correspondence: jatoliveira@uepg.br; Tel.: +55-42-32203044

Abstract: Cohesive Oxisols are a type of soil common in the Coastal Plateau in Brazil. These soils represent a challenge for agriculture and their study is fundamental to better land use. There have been a few studies on the porous system of cohesive soils on the micrometer scale. Our study aimed to provide a detailed analysis of the pore complexity of the cohesive horizon of a Brazilian Oxisol using 3D images (volumetric data reconstructed by 2D CT slices) and to correlate these parameters with soil physical–hydric attributes. For this purpose, images with two different resolutions were analyzed from multifractal, lacunarity, and entropy analyses. Additionally, a characterization of hydraulic properties was carried out based on a soil water retention curve (SWRC). No differences were observed between the resolutions for the different physical parameters analyzed. The lacunarity analysis showed a greater homogeneity of the pore system with pores grouped in clusters. The multifractal analysis showed fractal characteristics for the cohesive horizon, suggesting a more homogeneous pore distribution. The main results obtained from the SWRC showed a low available water content due to the predominance of ultramicropores. Overall, the results show a less complex pore system, indicating the presence of pores of small sizes, affecting the water retention and conduction through the soil.

Keywords: 3D image analysis; X-ray microtomography; Shannon entropy; lacunarity; pore architecture; cohesive horizon; soil pore system

Academic Editor: Hailong He

Received: 12 December 2024
Revised: 5 January 2025
Accepted: 13 January 2025
Published: 17 January 2025

Citation: Oliveira, J.A.T.d.; Pessoa, T.N.; Gaspareto, J.V.; Posadas, A.N.D.; Lourenço, A.L.F.; Libardi, P.L.; Pires, L.F. Characterization of the Pore Network of a Cohesive Oxisol Through Morphological and Pore Complexity Analyses. *Agriculture* **2025**, *15*, 200. https://doi.org/10.3390/agriculture15020200

1. Introduction

Cohesive soils are found in the Coastal Plateau in Brazil, occupying an area of approximately 200,000 km^2. These soils have peculiar characteristics when compared to other soils found in Brazil. These include a hard or extremely hard subsurface horizon when dry [1], which becomes friable when moist and is easily deformed [2]. As cohesive soils are in an extensive area close to the Brazilian coast, distributed from Rio de Janeiro to Amapá and have high agricultural potential, they are of great environmental and economic interest. However, the intrinsic characteristics and properties of these soils present a significant challenge for agricultural production [3,4]. Cohesive soils are generally characterized by a high soil bulk density (1.50–1.80 g cm^{-3}) and are generally unstable and susceptible to degradation [5–7]. In their dry state, the high soil bulk density of these soils prevents plant

roots from penetrating, and the roots usually found in cohesive horizons are either dead or underdeveloped [8]. Additionally, high soil bulk density affects water infiltration in the cohesive horizons, influencing the development of plant roots in the surface horizons [9].

Some Brazilian researchers have been investigating the physical characteristics of cohesive soils, with the objective of enhancing the utilization of this type of soil in agricultural activities. Lima et al. [10] analyzed the degrees of compaction of cohesive soils. They found that some of these soils did not present suitable agricultural conditions, especially in the harder cohesive horizons. Mota et al. [11] studied cohesive soils' morphometry and pore orientation, showing that rounded pores predominate. These soils have a suitable pore distribution, essential for agricultural cultivation; however, the cohesive horizons showed reduced total pore volume and amount of macropores. Schossler et al. [12] showed that cohesive soils can have good agricultural productivity when moisture conditions are favorable, even for soil bulk density values considered high. Queiroz et al. [13] mapped the moisture values at which the soil becomes cohesive. The friable or firm consistency of the soil was observed when the soil moisture was close to field capacity, and the soil became hard to extremely hard when the soil was in the air-dry condition. Menezes et al. [9] analyzed the functionality of the pore network of cohesive horizons, showing that their pores are less functional with low air permeability, length, and connection between pores. Low pore connectivity affects the soil's transport of gases and heat, impacting plant development.

The studies presented above are primarily based on the analysis of macroscopic soil properties and the investigation of two-dimensional (2D) images. Tools that make it possible to investigate the interior of soil samples without destroying them and in three dimensions (3D) can provide essential results on the physical characteristics of cohesive soils. X-ray microtomography (XCT) is a technique that enables the investigation of the internal structure of soil samples at the micrometer scale, thereby facilitating the study of soil pore characteristics and their functional properties [14–17].

Other recent advances have significantly enhanced the study of cohesive soils, enabling researchers to explore their microstructure, mechanical behavior, and interaction with external factors. Phalempin et al. [18] developed a method to correlate penetration resistance (PR) with gray values (GVs) obtained via XCT, focusing on loam and sand soils. Their study revealed that loam, being cohesive, showed stronger correlations between PR and GV, paving the way for creating 3D PR maps. These maps provide a detailed understanding of soil compaction and heterogeneity, offering practical applications in root–soil interaction studies and agricultural soil management [18]. Similarly, Liu et al. [19] combined triaxial compression tests with X-ray CT imaging to investigate how particle shapes affect soil fabric evolution under shear stress. Their findings demonstrated that cohesive soils develop distinct anisotropic patterns during deformation, offering insights into soil stability and structural integrity [19].

In agricultural contexts, XCT has proven to be a powerful tool for assessing soil health and management practices. For instance, Pereira et al. [20] used the technology to quantify potato cyst nematodes in cohesive soils, enabling precise detection of pest distributions without disturbing the soil structure. This method offers a promising avenue for integrating pest management with soil health assessments, as the non-destructive nature of XCT ensures accurate analysis while preserving the soil matrix. The study highlights the potential for combining XCT with AI-driven analysis for rapid and scalable agricultural applications [20].

While there have been numerous studies in which XCT was used to characterize soil pore architecture, the number of studies on cohesive soils is still limited. In addition to the morphological and geometric characterization of soil pores, 3D XCT images also make it

possible to ascertain the complexity of soil pores. This complexity has a direct impact on the dynamics of water and gases, affecting the retention, distribution, and infiltration of water in the soil [21–23].

Tools such as multifractal, lacunarity, and entropy analyses have been employed to characterize the complexity of porous systems, including soil [24–26]. According to the multifractal approach, a statistically self-similar measure can be expressed as a combination of interwoven fractal sets with matching scaling exponents. The combination of all the fractal sets results in the formation of a multifractal spectrum, which servers to reflect the diversity and heterogeneity of the variable under study. The multifractal technique has the advantage of not requiring any assumptions about the data following any particular distribution and allowing the multifractal parameters to be independent of the size of the objects under study [27]. The parameters provided by multifractal, lacunarity, and entropy analysis allow for the complexity of pores in localized regions to be determined, permitting inferences to be made about the impact of this complexity on the functionality of soil pores.

In recent years, XCT images have been used to analyze soil pore complexity using multifractality. Soto-Gómez et al. [28] analyzed the effect of different soil managements on pore complexity, showing that plant roots and the action of soil fauna influence soil multifractality. These authors also observed different levels of complexity in the soil pore network. Martinez et al. [29] used multifractal analysis to study variations in macroporosity with soil depth, showing low spatial variability in the horizontal direction but complex structures at depth. Ju et al. [30] showed that contrasting soils have different multifractal characteristics, with pore connectivity and pore number significantly influencing multifractal parameters. Torre et al. [31] evaluated the effect of different soil management types on pore complexity using multifractal analysis. The authors showed that more invasive managements that destroy soil aggregates tend to present a weak multifractal nature. In Tarquis et al. [32], the importance of porosity in the complexity of the soil pore system was verified, observing that increases in porosity tend to reduce the complexity of the pore space. The authors also analyzed the influence of the image binarization process on the multifractal analysis.

Cohesive soils cover Ultisols and Oxisols spread over a large area of Brazil's coastal territory. Although previous studies have evaluated the physical attributes of cohesive soils, the complexity of their pore systems at the micrometric scale remains insufficiently understood. This lacuna in knowledge is significant, given the economic importance of this soil type for agriculture, particularly in northeastern Brazil. To address this, we analyzed the pore system of cohesive soil using XCT combined with multifractal analysis, lacunarity, entropy, and hydraulic properties derived from the soil water retention curve (SWRC). Our study specifically examined images at two different resolutions to evaluate the influence of scale and pore size on the results. This research may help fill part of this knowledge gap by offering a deeper understanding of the complexity of the pore system, which is essential for promoting the sustainable and ecological management of this vital natural resource.

2. Materials and Methods

2.1. Experimental Area and Soil Sampling

The soil utilized in this study was classified as Xanthic Kandiustox [33], located in Cruz das Almas, Bahia, Brazil (12°39′24.78″ S, 39°05′09.26″ W—Figure A1), climate type of Aw (tropical zone with dry winter) [14], and parental material related to sediments of Barreiras Formation (Tabuleiros Costeiros). The particle size distribution of this Oxisol is composed of a higher amount of sand, a lower amount of silt, and clay, characteristic of a sandy-loamy clay texture. The clay mineral composition indicates that the mineral kaolinite constitutes 78% of the clay fraction, while 16% is composed of the iron oxide

goethite. Table 1 presents soil bulk density (ρ), total porosity (β), and other physical–hydric attributes.

Table 1. Physical–hydric attributes of the Xanthic Kandiustox studied.

Physical Attributes	Unit	Value
Clay	%	29.50
Silt	%	1.58
Very coarse sand	%	7.95
Coarse sand	%	22.10
Medium sand	%	21.38
Fine sand	%	13.85
Very fine sand	%	3.64
Soil bulk density (ρ)	g cm^{-3}	1.68 ± 0.02
Particle density (ρ_s)	g cm^{-3}	2.73 ± 0.01
Total porosity (β)	cm^3 cm^{-3}	0.38 ± 0.01
Saturated hydraulic conductivity (K_{sat})	mm h^{-1}	82.87 ± 0.26

Mean values and their respective standard deviation. The methods are described in Teixeira et al. [34] and Pessoa et al. [14].

Soil samples were collected from the surface of the cohesive Bw horizon (0.38 m) of a pit in a sub-evergreen tropical forest (Figure A1). The samples were collected during the summer period and under field moisture conditions. However, due to the difficulty of collecting undisturbed samples in the cohesive horizon under natural moisture and high hardening, a wetting procedure was performed before sampling. After approximately two hours of the wetting process, the blocks and other soil samples were then collected.

For XCT scanning, undisturbed soil blocks were sampled using plastic containers with dimensions of ≈0.33 × 0.22 × 0.10 m (see Figure A1), i.e., between a 0.38 and 0.60 m soil depth. The collected soil blocks were air-dried in the laboratory, separated into small pieces from the surface of blocks, and sculpted to obtain approximately cubic subsamples with height and diameter dimensions of 0.020 × 0.020 m and 0.020 × 0.010 m (Figure A1). For the determination of the soil bulk density, total porosity, and saturated hydraulic conductivity, samples were collected (NS = 10, number of samples) with cylindrical rings (0.07 m of height × 0.075 m of diameter) using an Uhland soil sampler.

Furthermore, additional undisturbed soil samples (0.05 m of height × 0.05 m of diameter) were collected (NS = 4; totaling 40 samples) using a type Uhland sampler for the determination of the soil water retention curve (SWRC) and soil physical–hydric attributes from SWRC data. Disturbed soil samples were also collected in five replicates (NS = 5) for soil attributes characterization (e.g., particle size distribution and particle density).

2.2. Sample Imaging

The samples air-dried were scanned using an X-ray benchtop Skyscan 1172 (Bruker micro-CT®, Kontich, Belgium) at an energy of 100 keV. A filter composed of aluminum (Al) and copper (Cu) was utilized to harden the beam, reduce beam hardening artifacts, and enhance the image quality high-density and heterogeneous materials such as soil samples. To obtain a voxel size of 15 µm for larger samples (0.020 × 0.020 m) and 9 µm for smaller samples (0.020 × 0.010 m), adjustments were made to the camera during the image scanning process. The projections were conducted in steps of 0.2° from 0 to 180°, resulting in a total of 940 projections for each sample. The 3D image reconstruction was performed using the software NRecon® 1.4.4 (Bruker microCT®, Kontich, Belgium). The volume of interest (VOI) for both resolutions (S_R1 = 9 µm and S_R2 = 15 µm) was 400 × 400 × 400 voxels (S_R1 = 3.6^3 mm^3 × 3 replicates and S_R2 = 6^3 mm^3 × 5 replicates).

2.3. Quantification of Physical and Morphometric Properties Analyzed Using 3D Imaging

The distribution patterns of pores within a porous network reflect the degree of heterogeneity in pore clustering. This heterogeneity can be quantified using a physical property known as lacunarity.

In the context of 3D image reconstruction, lacunarity (Equation (1)) relates the number s of black voxels (pores) contained within the ε size box with the probability $P(s,\varepsilon)$ of quantification of these voxels [24,26,35,36].

$$\Lambda(\varepsilon) = \frac{\sum_s s^2 P(s,\varepsilon)}{\left[\sum_s sP(s,\varepsilon)\right]^2}, \tag{1}$$

Porous media with a high pore similarity in their networks typically exhibit overlapping lacunarity curves. Thus, the process of deriving lacunarity according to Equation (2) enables better differentiation of these curves by analyzing their maximum and minimum inflection points [37].

$$\frac{d\ln\Lambda(\varepsilon)}{d\ln\varepsilon} = \frac{\ln\Lambda(\varepsilon_{i+1}) - \ln\Lambda(\varepsilon_{i-1})}{\ln\varepsilon_{i+1} - \ln\varepsilon_{i-1}} \tag{2}$$

where $\Lambda(\varepsilon)$ represents the lacunarity and i indicates each slope point on the lacunarity curve.

The probability $P(s, \varepsilon)$ expresses the ratio of the number of frequencies of mass distribution $n(s, \varepsilon)$ to the total number $N(\varepsilon)$ with size ε (Equation (3)).

$$P(s,\varepsilon) = \frac{n(s,\varepsilon)}{N(\varepsilon)}, \tag{3}$$

Using Equation (1), a script was developed in a Matlab® [38] environment to quantify 3D lacunarity data in images of cohesive soil samples using the box-counting method. The cubic box sizes used were as follows: 1, 2, 4, 5, 8, 10, 16, 20, 25, 40, 50, 80, 100, 200, and 300.

Analyses using 3D multifractal approaches for the reconstructed sample volumes were conducted by constructing multifractal spectra with the NASS (Non-linear Analysis Scaling System) software. NASS applies Equations (4) and (5) to calculate multifractal spectra with statistical moments (q values) ranging from -0.4 to 2.0 in regular 0.1 increments, and with cubic box sizes (ε) of 4, 8, 10, 20, 40, 50, 80, 100, and 200 [26,28,39–41].

$$f(\alpha(q)) = \lim_{\varepsilon\to 0} \frac{\sum_i \mu_i(q,\varepsilon)\log_e \mu_i(q,\varepsilon)}{\log_e \varepsilon}, \tag{4}$$

$$\alpha(q) = \lim_{\varepsilon\to 0} \frac{\sum_i \mu_i(q,\varepsilon)\log_e P_i(\varepsilon)}{\log_e \varepsilon}, \tag{5}$$

where μ_i is the partition function or normalized measure, q represents the statistical moment of the distribution, $f(\alpha(q))$ is the singularity spectrum of the distribution, $\alpha(q)$ refers to the singularity points or the Lipschitz-Hölder exponent, and $P_i(\varepsilon)$ denotes the probabilities of counting pores within a box of size ε.

The NASS software also quantifies the physical property of normalized Shannon entropy, which expresses the uncertainty or inaccuracy in the detection of voxels associated with the pore within the cubic box of size ε^3 (Equation (6)). Normalized Shannon entropy is a physical property dependent on the scale and, thus, is very sensitive in detecting heterogeneous subtlety in the porous nets [24,26,36,42].

$$H^*(\varepsilon) = \frac{H(\varepsilon)}{H_M(\varepsilon)} = -\frac{\sum_{i=0} P_i(\varepsilon)\log P_i(\varepsilon)}{\log(\varepsilon^3+1)}, \tag{6}$$

In the case of normalized Shannon entropy, additional cubic boxes equal to 1–10, 16, and 25 were implemented for better detail of this physical property.

2.4. Soil Water Retention Curve (SWRC) and Physical–Hydric Attributes

The soil water retention curve (SWRC) was determined using Haines funnels and Richards pressure chambers [43]. The matric potentials of −2, −4, −6, and −8 kPa were determined by employing Haines funnels and those of −10, −30, −100, −300, −500, and −1500 kPa by utilizing Richards pressure chambers. Each point of the SWRC was determined using four undisturbed soil samples (NS = 4), totaling 40 samples, to obtain the whole range of the SWRC. The software used in the data fit was the Table Curve 2D, which is known for its efficiency in eliminating endless trial and error by automating the curve fitting using Equation (7) proposed by van Genuchten [44]:

$$\theta = \theta_r + \frac{(\theta_s - \theta_r)}{\left[1 + (\alpha|\psi_m|)^n\right]^m} \quad (7)$$

where θ is the volumetric soil water content ($cm^3\ cm^{-3}$), ψ_m is the matric potential (m), θ_s is the saturated soil water content ($cm^3\ cm^{-3}$), θ_r is the residual soil water content ($cm^3\ cm^{-3}$), and α, m, and n are empirical parameters.

The parameters θ_s, θ_r, α, m, and n were obtained from Equation (7), considering the restriction $m = 1 - (1/n)$. The hydraulic conductivity was determined as a function of the effective relative saturation (ω). Initially, the relative hydraulic conductivity was calculated by the van Genuchten model (Equation (8)) based on Mualem's model [45]:

$$K_r = \omega^l \left[1 - \left(1 - \omega^{1/m}\right)^m\right]^2 \quad (8)$$

where l is an empirical parameter considered 0.5 by Mualem [45].

The effective relative saturation (ω) was calculated as $(\theta - \theta_r)/(\theta_s - \theta_r)$. K($\omega$) was estimated by the product K_{sat}.Kr(ω). K_{sat} was measured from the undisturbed soil samples by the constant head permeameter method using a Mariotte flask and deionized water. Once a steady-state condition was reached, the Darcy–Buckingham equation was applied [43,46]. Further details regarding the equations and soil hydraulic determinations can be found in Pessoa and Libardi [47].

The soil pore size distribution was estimated from the equivalent radius (r) and the pore size radius classification adapted from Brewer [48], which includes macropores (r > 40 μm), mesopores (15–40 μm), micropores (2.5–15 μm), and ultramicropores (<2.5 μm). The field capacity (FC) was considered as the volumetric soil water content (θ, $cm^3\ cm^{-3}$) corresponding to ψ_m = −10 kPa, the permanent wilting point (PWP) was considered as θ corresponding to ψ_m = −1500 kPa, and the available water content (AWC) was obtained by the difference between FC and PWP. The FC was defined as the soil water content at ψ_m = −10 kPa since it is a soil with a high sand fraction.

3. Results and Discussion

3.1. 3D Lacunarities, 3D Multifractal Spectra, and Normalized Shannon Entropy

The 3D lacunarity analysis (Figure 1a) shows no significant differences (as indicated by error bars) between the lacunarity values at the two resolutions evaluated. Lacunarity is a geometric measurement of objects or structures [24,49]. Lower lacunarity values are usually associated with more homogeneous porous media, while higher values indicate more heterogeneous media.

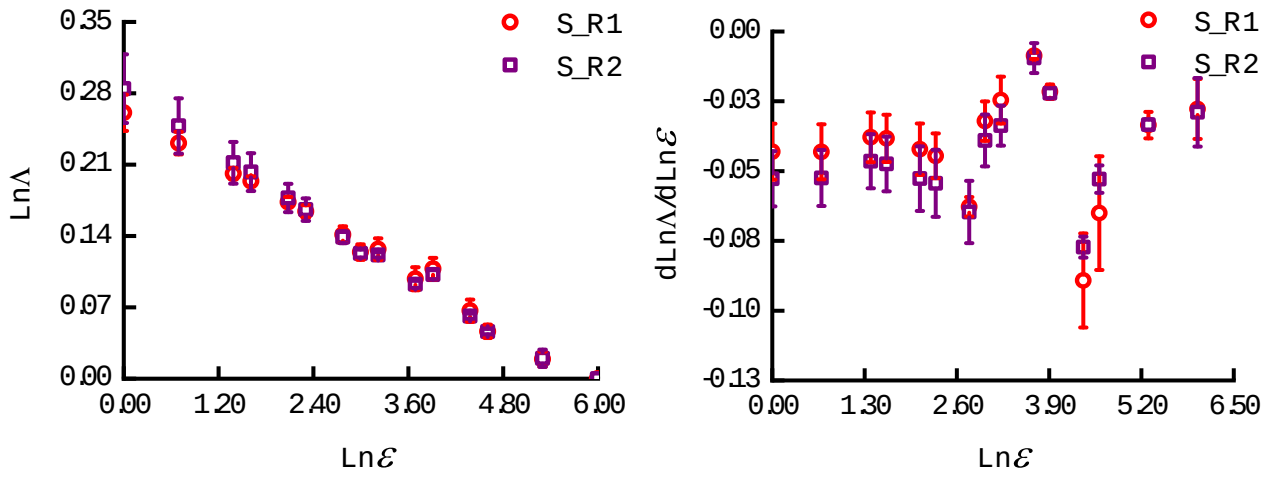

(**a**) (**b**)

Figure 1. (**a**) 3D lacunarities and (**b**) their derivatives for two different resolutions.

In porous media such as soil, increases in the value of lacunarity are related to the appearance of larger pores [24]. Therefore, this parameter can also be used to infer the spatial pore distributions [36]. Our lacunarity results are close to those quantified by Lee and Lee [36] in glass spheres and irregularly crushed silica gel particles with a porosity between 26% and 27%. In accordance with the aforementioned authors, this linearity behavior in lacunarity curves is attributed to the presence of intermediate pores within the sample's porous systems. This finding was also corroborated by the observation of homogeneity in our porous networks and the linearity of our lacunarity curves (Figures 1a and 2a,b).

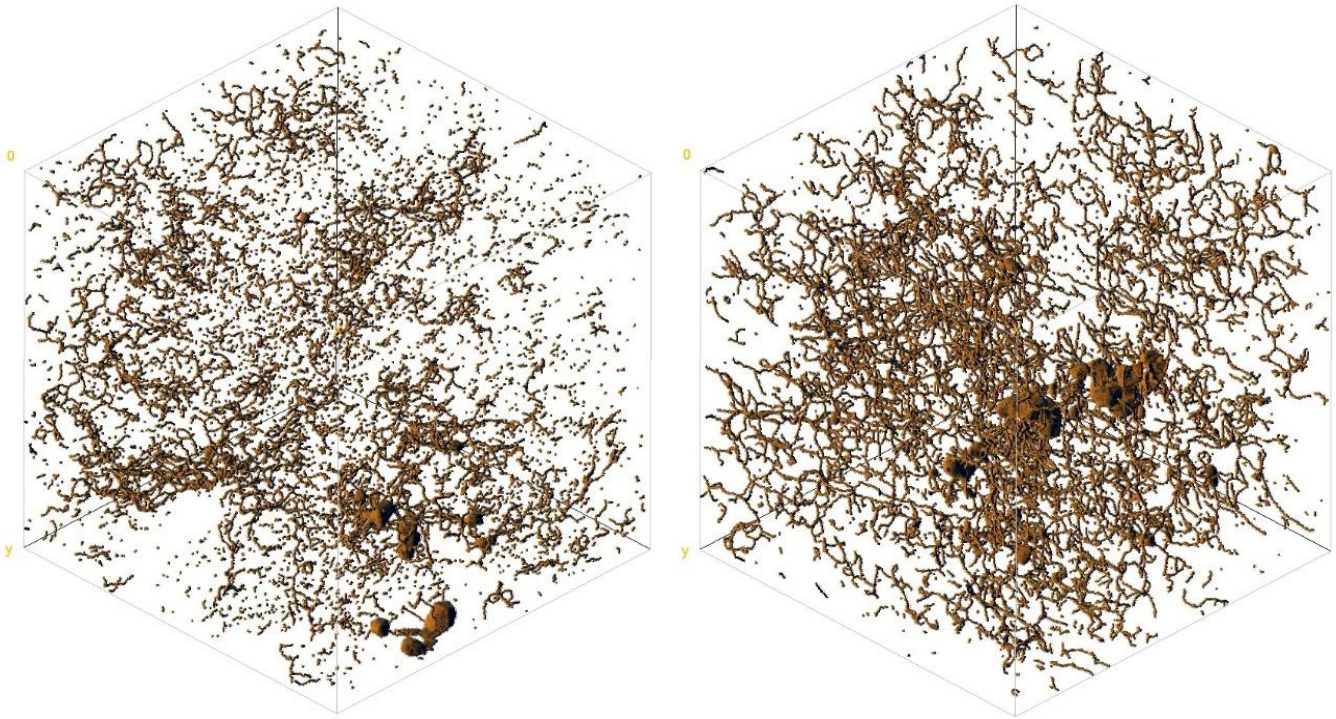

(**a**) (**b**)

Figure 2. Cohesive soil pore network at two different resolutions. (**a**) S_R1 = 9 µm. (**b**) S_R2 = 15 µm.

Zeng et al. [50] presented values of $\Lambda(\varepsilon)$ for undisturbed soil samples relatively close to ours and related the dispersion of lacunarity to the variability of the bulk density (ρ) of their samples. By employing the value of ρ = 1.68 ± 0.02 g cm^{-3} as presented in Table 1

in conjunction with the results of $\Lambda(\varepsilon)$, our results diverge from those of Zeng et al. [50]. This can be attributed to two factors: firstly, the relatively narrow standard deviations for ρ, and secondly, the presence of 30% clay in this cohesive soil. Given the above, our low lacunarity values allow us to state that the porous network of this cohesive Oxisol are quite homogeneous.

High values of $\Lambda(\varepsilon)$ were reported by de Oliveira et al. [26] when studying an Oxisol under different types of management. According to the authors, these values demonstrate the heterogeneity and dispersiveness of pores within the investigated porous systems. Given the above, it is evident that our values are lower than those of these authors, revealing that these porous systems are more homogeneous with the less dispersed pore clusters (see Figure 2a,b). This result is consistent with the characteristics and properties typically observed in a cohesive horizon, which is a soil with greater density, lower macroporosity, and greater soil resistance to penetration [10,11,51].

Inspection of the first derivatives of the lacunarity curves (Figure 1b) for each resolution reveals no significant differences, as expected, given that both curves derive from $\Lambda(\varepsilon)$. The derivation process provides valuable information about the variability in the spatial distribution of clusters across scales, as evidenced by the maximum and minimum inflection points [37]. Compared with the results of the derivatives presented by de Oliveira et al. [26], we note that the values of the two minimum inflection points (Figure 1b) found indicate low diversity of pore size clusters for both resolutions (S_R1 and S_R2), as visually shown in the pore networks in Figure 2a,b.

Examining the multifractal spectra (Figure 3a,b), strong similarities are observed between the replicates and, mainly, between the resolutions. This finding allows us to conclude that the porous systems of these samples are fractals (corroborated by $D_{q's}$—discussion below). Multifractal porous systems are typically observed in soils that have undergone intensive management practices, which have the effect of modifying both the soil structure and the soil pore system [31]. However, this is not the case for the studied cohesive Oxisol, which was collected under native forest conditions without soil management. Porous systems with fractal behaviors are typically less complex and more homogeneous than multifractal systems, as they are distinguished by a single fractal dimension [30,52]. Studies conducted on Oxisols by Vidal-Vazquez [52] revealed that the multifractal spectra exhibited fractal or multifractal behavior along transects for sand, silt, and clay contents, especially in the transect with less clay content, and close to that presented on Table 1.

Approximate multifractal spectra in amplitude values of $f(\alpha(q))$ versus α can be seen in de Oliveira et al. [26]. However, the porous systems of the samples of these authors appear to be multifractal, opposite to what was observed here (see Figure 3a,b). The researchers mention that they found low variability and heterogeneity in the spatial distributions of the pores. Although spectra amplitudes are close, the asymmetries of our spectra curves compared to these authors are more symmetrical and with a small tendency to the left side of the spectra, thus reinforcing the homogeneity and fractality of the porous system investigated here.

The 3D normalized Shannon entropies (Figure 4) for 9 µm and 15 µm resolutions show no observable differences. This type of entropy is highly sensitive to the quantification of pore structure organization, enabling inferences about their complexity as a function of scale. Thus, $H^*(\varepsilon)$ represents the pore occupancy rate within cubic box size ranges, reflecting variations in the quantity of these elements. Accordingly, a lower $H^*_{maximum}(\varepsilon)$ value for an optimal cubic box size indicates a lower probability $P(s, \varepsilon)$ of accounting for large-caliber pores (pores with larger diameters) [24,26].

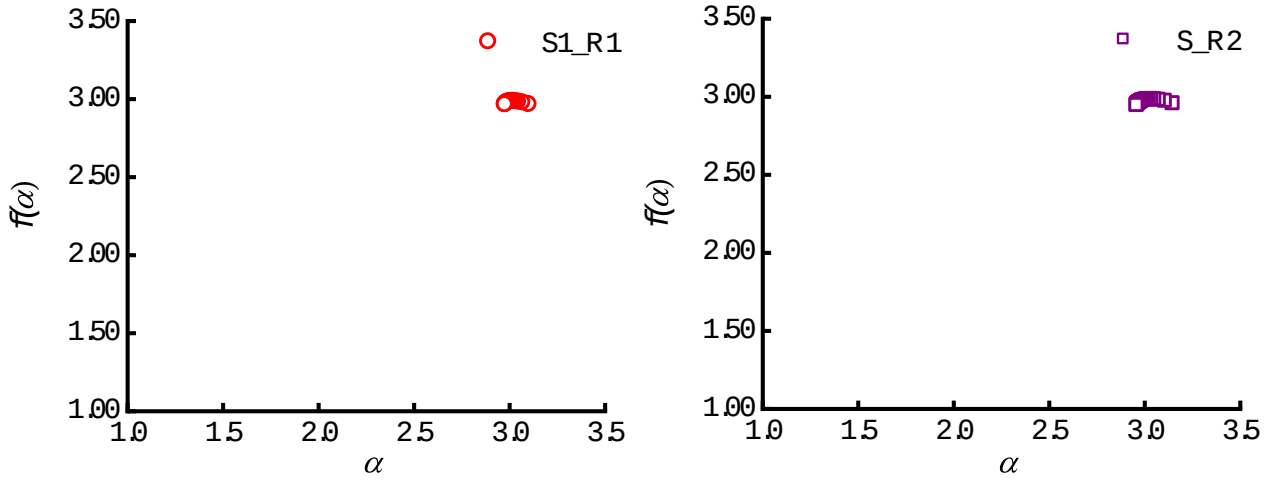

(**a**) (**b**)

Figure 3. Multifractal spectra at two different resolutions representing the replicates: (**a**) sample 1 with a lower resolution and (**b**) sample 2 with a higher resolution. Both samples exhibit homogeneous pore size distributions concentrated in a cluster pattern.

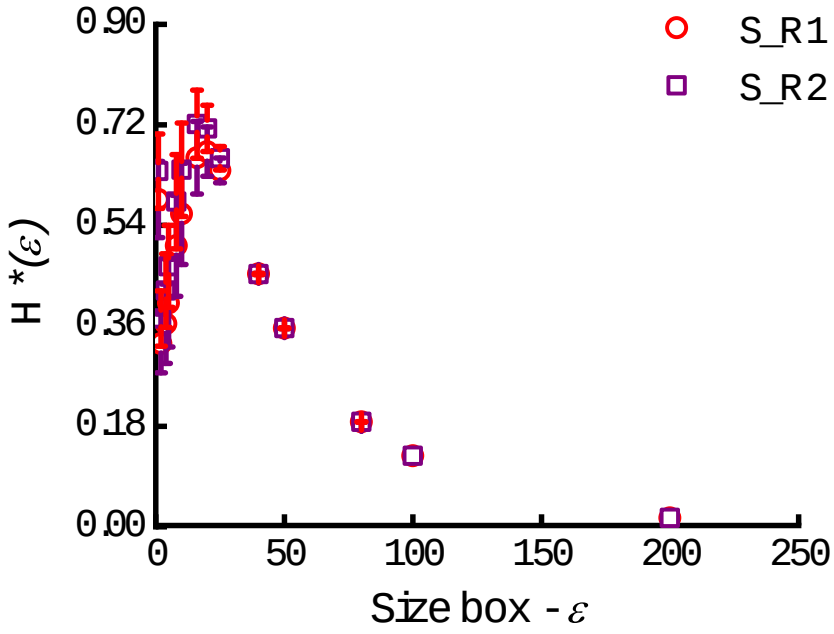

Figure 4. The 3D normalized Shannon's entropies of two different resolutions.

$H^*(\varepsilon)$, also referred to as the configurational entropy of the system, can be used to quantify the degree of disorder observed in porous systems within soil samples [36]. Analyzing Figure 4, we observe that the peaks of $H^*_{maximum}(\varepsilon)$ for both resolutions are lower compared to those reported by de Oliveira et al. [26]. This observation suggests a reduction in the degree of disorder within the pore networks, thereby confirming an increase in their overall homogeneity.

These results of lower numerical values found for the 3D normalized Shannon's entropies compared to the literature once again reaffirm the fractality (multifractal spetrum-Figure 3a,b) of the porous structure in this cohesive soil at the investigated resolutions. This is evidenced by the prevalence of pores with small diameter sizes through the SWRC (ultramicropores-Figures 2 and 5a,b) and the smoothed shape of the SWRC.

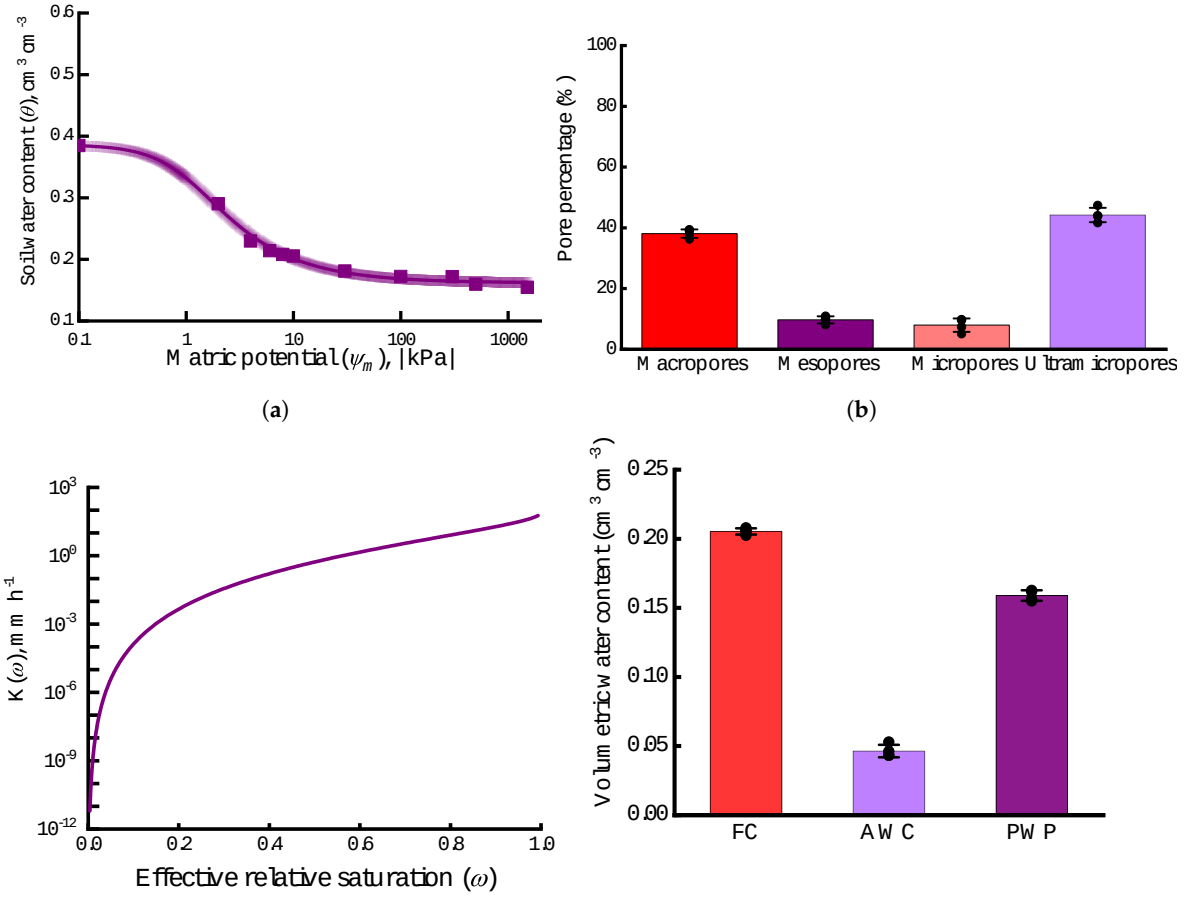

Figure 5. (**a**) Soil water retention curves, (**b**) pore size classes, (**c**) hydraulic conductivity, and (**d**) field capacity (FC), available water content (AWC), and permanent wilting point (PWP).

3.2. Multifractal Analysis Versus Soil Physical–Hydric Behavior

The main findings of multifractal analysis indicated a porous system characterized by fractal behavior. This implies that the pore network between the different scales is constant, reflecting in more homogeneity in the structural soil conditions, affecting the soil physical-hydric attributes. This behavior may be related to the low amount of clay present in this cohesive soil, since the fractal dimension increases with increasing clay amount [53]. The soil water retention curve (SWRC) evidences the data fitted by the van Genuchten model (lines) and the points observed with their respective confidence intervals (points and shaded area along the curve) (Figure 5a). The SWRC data were well-fitted by Equation (7), as shown by the low **RMSE** and high R^2 values (Table 2). It is possible to observe the smoothness of the curve without abrupt changes in the variation of water content and the low variability in the observed data among the measured matric potentials (Figure 5a). The gradual transition between each point measured suggests a good pore size continuity, controlled by the fractal porous system, as the fractal dimension establishes a good relationship between soil structure and hydraulic properties [53,54]. In general, the heterogeneous porous system presents higher inflection points in the SWRC, influencing the greater variations of the pore size distribution [55].

Table 2. Soil water retention curve parameters from the fitting of data to Equation (7), R^2, and **RMSE**.

θ_s	θ_r	α	n	m	RMSE	R^2
$cm^3\ cm^{-3}$		kPa^{-1}				
0.386	0.162	0.930	1.776	0.437	1.97×10^{-4}	0.956

The soil pore size (radius) obtained from the SWRC indicates that the soil porous system is dominated by ultramicropores (pores with equivalent radii < 2.5 µm) and macropores (pores with equivalent radii > 40 µm), followed by mesopores and micropores (Figures 2a,b and 5b). It is important to highlight the low variability in the standard deviation, as the points are tightly clustered around each deviation bar, indicating low variability among the replicates. This provides further evidence in support of the hypothesis that the soil exhibits minimal variation in porosity (Figure 5b). The predominant pore sizes found are responsible for the movement of water and air and water retention, respectively. The predominance of small pore sizes reinforces the tendency of fractality of the porous system of this cohesive Oxisol [26]. The higher percentages of small pores resulted in medium values found for the saturated hydraulic conductivity (Ksat) (Table 1) when compared to other typical Brazilian Oxisols, which exhibited higher permeability and higher proportions of conduction pores, such as macropores and mesopores [14,47]. Figure 5c shows the hydraulic conductivity as a function of effective relative saturation, K(ω), evidencing the capacity of water conduction with the changes in the saturation. At the beginning and middle of the curve, relatively low values of K ($\approx 10^{-10}$ to 10^{0} mm h^{-1}) can be observed, which are probably due to lower water-connecting pores, limiting the water flux. As the soil water content increases, i.e., the effective relative saturation approaches 1, the hydraulic conductivity increases to $\approx 10^{2}$ mm h^{-1}.

The distribution of pores (PSD) in the soil matrix is crucial for interactions between the solid, liquid, and gaseous phases, influencing the spatial and temporal evolution of water movement processes in the soil [56]. The PSD determines the soil's physical–hydric behavior, affecting its agricultural potential. Homogeneous porous systems favor the presence of macropores throughout the soil profile, facilitating water transport. In contrast, heterogeneous systems, with both macropores and micropores, enable a uniform water distribution. Therefore, understanding the spatial distribution of pores in the soil is essential for the efficient use of water by plants, and the multifractal technique forms the basis for applying precision agriculture concepts.

Figure 5d illustrates the influence of pore size distribution on physical–hydric attributes that are essential for plant growth and water utilization in agricultural systems. The higher water content corresponding to FC and PWP is associated with the higher percentages of macropores and ultramicropores (Figure 5a,b) of the soil, respectively (Figure 5b). This is reflected in the low available water content (AWC) for plants found in this cohesive Oxisol (Figure 5d), which affects the capacity of this soil to support the plant development duo to subsurface (i.e., cohesive horizon). The tendency for a lower AWC and a fractal porous system can result in a decrease in the resilience of soil in retaining water and nutrients for plant development in agricultural systems [57]. In this case, the agricultural management of this cohesive Oxisol may necessitate the implementation of short intervals of irrigation due to the fractal characteristics of the porous system, in addition to the high variation observed in the behavior of hydraulic conductivity (Figure 5c). In agricultural systems, multifractal porous systems can facilitate greater structural variability and a heterogeneous distribution of pore sizes, thereby promoting gradual conduction and water retention, as well as the formation and additional channels for gases and water fluxes. These characteristics may promote a more sustainable plant development in the context

of water deficits, environmental variations, and the enhancement of the management of agricultural systems.

4. Conclusions

This study assessed the complexity of the pore system of the cohesive horizon of an Oxisol. The results show that the soil has a slightly complex pore system and does not exhibit multifractal characteristics. This result is mainly associated with the higher soil bulk density found in the cohesive horizon and the more significant percentage of small pores (ultramicropores). The lower pore complexity associated with smaller pores affects pore connectivity, directly impacting water conduction, as demonstrated in our paper. Pore size distribution is a valuable indicator of soil physical quality. It can be used to evaluate sustainable practices in agricultural soils, with the multifractal technique serving as a powerful tool for its characterization. The 3D lacunarity results indicated the presence of a more homogeneous pore network, reinforcing the existence of pores in a narrower range of sizes. The 3D Shannon entropy data also showed the homogeneity of the pore system, confirming the existence of a pore network with fractal characteristics. One consequence of this homogeneity was that a significant amount of water was still retained in the smaller pores in the soil, even though the soil contained a significant amount of sand. As a result, the amount of water available to the plants was greatly reduced. Another objective of this paper was to analyze images with two different resolutions, which involves accessing different pore sizes through microtomography. The results showed no significant differences between the samples for the different resolutions associated with the more homogeneous pore network in the cohesive horizon. Overall, this study shows that pore complexity is highly influenced by the cohesive horizon, directly impacting water retention and conduction through the soil. However, we stress the need for further studies using other types of cohesive soils to see if the homogeneity observed in our study is also seen in more clayey cohesive soils.

Author Contributions: Conceptualization, L.F.P.; methodology, J.A.T.d.O., T.N.P. and J.V.G.; software, A.N.D.P., A.L.F.L. and T.N.P.; Validation, J.A.T.d.O., A.N.D.P. and A.L.F.L.; formal analysis, J.A.T.d.O., J.V.G. and T.N.P.; investigation, J.A.T.d.O. and T.N.P.; resources, L.F.P., A.N.D.P., P.L.L. and T.N.P.; writing—original draft preparation, J.A.T.d.O., T.N.P. and L.F.P.; writing—review and editing, A.N.D.P., A.L.F.L., J.A.T.d.O., P.L.L. and T.N.P.; project administration, L.F.P., P.L.L. and T.N.P.; funding acquisition, L.F.P., A.N.D.P. and T.N.P. All authors have read and agreed to the published version of the manuscript.

Funding: This research was partially funded by "Conselho Nacional de Desenvolvimento Científico e Tecno-lógico" (CNPq) (Grants 303950/2023-4, 404058/2021-3 and 140126/2017-1) and "Coordenação de Aperfeiçoamento de Pessoal de Nível Superior" (CAPES) (Grant Code 001).

Institutional Review Board Statement: Not applicable.

Data Availability Statement: All data are available upon reasonable request to jatoliveira@uepg.br.

Acknowledgments: We acknowledge Carlos Manoel Pedro Vaz and Embrapa Instrumentation for support in scanning images with an X-ray benchtop Skyscan 1172.

Conflicts of Interest: Authors Adolfo N. D. Posadas and André L. F. Lourenço were employed by the company AgriEntech Ltda. The invited authors, associates of Agrientech, a private company, have no financial interests. Their commercial work involves multispectral image processing for the detection of plagues and diseases in agricultural fields. The contribution to this study is about their previous academic expertise in multifractal image processing techniques.

Appendix A

Figure A1 illustrates the location of the city where the cohesive soil samples were collected, along with the sampling procedures.

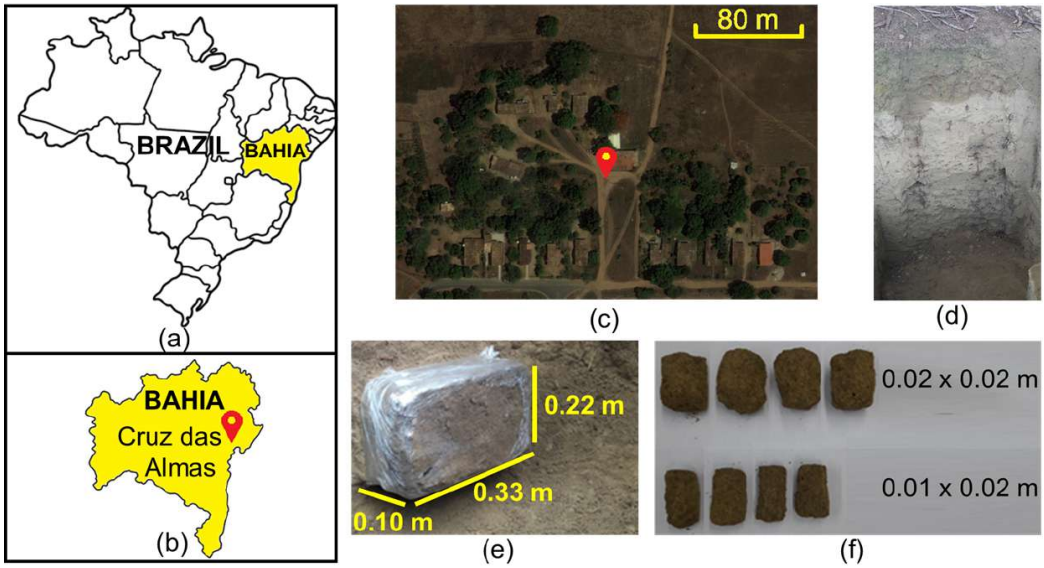

Figure A1. (**a**) Location of the state and (**b**) city on the map of Brazil. (**c**) A visual representation of the city where the soil samples were collected. (**d**) Cohesive soil profile trench. (**e**) Cohesive soil block of the sampled profile. (**f**) Subsamples of approximately cubic soil samples of different sizes.

References

1. Giarola, N.F.B.; Silva, A.P.d. Conceitos sobre solos coesos e hardsetting. *Sci. Agric.* **2002**, *59*, 613–620. [CrossRef]
2. Jacomine, P. Distribuição geográfica, características e classificação dos solos coesos dos Tabuleiros Costeiros. In *Reunião Técnica Sobre Solos Coesos dos Tabuleiros Costeiros, Cruz das Almas*; 1996; pp. 13–26. Available online: https://www.scielo.br/j/sa/a/sjLYWg3QvZPbtLgGMTtqdZQ/?format=pdf&lang=pt (accessed on 11 December 2024).
3. Lima Neto, J.d.A.; Ribeiro, M.R.; Corrêa, M.M.; Souza-Júnior, V.S.d.; Araújo Filho, J.C.d.; Lima, J.F.W. Atributos químicos, mineralógicos e micromorfológicos de horizontes coesos de latossolos e argissolos dos tabuleiros costeiros do estado de Alagoas. *Rev. Bras. Ciênc. Solo* **2010**, *34*, 473–486. [CrossRef]
4. Lima, R.P.; Rolim, M.M.; Oliveira, V.S.; Silva, A.R.; Pedrosa, E.M.R.; Ferreira, R.L.C. Load-bearing capacity and its relationships with the physical and mechanical attributes of cohesive soil. *J. Terramech.* **2015**, *58*, 51–58. [CrossRef]
5. Gomes, J.B.V.; Araújo Filho, J.C.; Vidal-Torrado, P.; Cooper, M.; Silva, E.A.d.; Curi, N. Cemented Horizons and Hardpans in the Coastal Tablelands of Northeastern Brazil. *Rev. Bras. Ciênc. Solo* **2017**, *41*, e0150453. [CrossRef]
6. Corrêa, M.M.; Ker, J.C.; Barrón, V.; Torrent, J.; Curi, N.; Torres, T.C.P. Caracterização física, química, mineralógica e micromorfológica de horizontes coesos e fragipãs de solos vermelhos e amarelos do ambiente Tabuleiros Costeiros. *Rev. Bras. Ciênc. Solo* **2008**, *32*, 297–313. [CrossRef]
7. Pessoa, T.N.; Bovi, R.C.; Nunes, M.R.; Cooper, M.; Uteau, D.; Peth, S.; Libardi, P.L. Clay mineral composition drives soil structure behavior and the associated physical properties in Brazilian Oxisols. *Geoderma Reg.* **2024**, *38*, e00837. [CrossRef]
8. Cavalcanti, R.Q.; Rolim, M.M.; de Lima, R.P.; Tavares, U.E.; Pedrosa, E.M.; Gomes, I.F. Soil physical and mechanical attributes in response to successive harvests under sugarcane cultivation in Northeastern Brazil. *Soil Tillage Res.* **2019**, *189*, 140–147. [CrossRef]
9. Menezes, A.S.; Alencar, T.L.; Assis Júnior, R.N.; Toma, R.S.; Romero, R.E.; Costa, M.C.G.; Cooper, M.; Mota, J.C.A. Functionality of the porous network of Bt horizons of soils with and without cohesive character. *Geoderma* **2018**, *313*, 290–297. [CrossRef]
10. Lima, H.V.d.; Silva, Á.P.d.; Giarola, N.F.B.; Imhoff, S. Index of soil physical quality of hardsetting soils on the brazilian coast. *Rev. Bras. Ciênc. Solo* **2014**, *38*, 1722–1730. [CrossRef]
11. Mota, J.C.A.; Menezes, A.S.; do Nascimento, C.D.V.; de Alencar, T.L.; de Assis Júnior, R.N.; Toma, R.S.; Romero, R.E.; Costa, M.C.G.; Cooper, M. Pore shape, size distribution and orientation in Bt horizons of two Alfisols with and without cohesive character from Brazil. *Geoderma Reg.* **2018**, *15*, e00197. [CrossRef]
12. Schossler, T.R.; Mantovanelli, B.C.; de Almeida, B.G.; Freire, F.J.; da Silva, M.M.; de Almeida, C.D.G.C.; Freire, M.B.G.d.S. Geospatial variation of physical attributes and sugarcane productivity in cohesive soils. *Precis. Agric.* **2019**, *20*, 1274–1291. [CrossRef]

13. dos Santos Queiroz, A.; dos Santos Dias, C.T.; da Silva Lopes, A.; do Nascimento, Í.V.; de Sousa Oliveira, L.; de Almeida, B.G.; de Araújo Filho, J.C.; da Silva Souza, L.; e Silva, M.B.; Romero, R.E. Water content as a deterministic factor in the assessment of cohesive character in soils of Coastal Tablelands (Northeast, Brazil). *Geoderma Reg.* **2023**, *32*, e00600. [CrossRef]
14. Pessoa, T.N.; Cooper, M.; Nunes, M.R.; Uteau, D.; Peth, S.; Vaz, C.M.P.; Libardi, P.L. 2D and 3D techniques to assess the structure and porosity of Oxisols and their correlations with other soil properties. *CATENA* **2022**, *210*, 105899. [CrossRef]
15. Pires, L.F.; Ferreira, T.R.; Cássaro, F.A.M.; Cooper, H.V.; Mooney, S.J. A Comparison of the Differences in Soil Structure under Long-Term Conservation Agriculture Relative to a Secondary Forest. *Agriculture* **2022**, *12*, 1783. [CrossRef]
16. Zhang, Y.; Wang, L.; Zhang, W.; Zhang, Z.; Zhang, M. Quantification of Root Systems and Soil Macropore Networks Association to Soil Saturated Hydraulic Conductivity in Forested Wetland Soils. *Forests* **2023**, *14*, 132. [CrossRef]
17. Li, Q.; Qian, Y.; Wang, Y.; Peng, X. The Relation between Soil Moisture Phase Transitions and Soil Pore Structure under Freeze–Thaw Cycling. *Agronomy* **2024**, *14*, 1608. [CrossRef]
18. Phalempin, M.; Rosskopf, U.; Schlüter, S.; Vetterlein, D.; Peth, S. Can we use X-ray CT to generate 3D penetration resistance data? *Geoderma* **2023**, *439*, 116700. [CrossRef]
19. Liu, J.; Leung, A.K.; Jiang, Z.; Kootahi, K.; Zhang, Z. X-ray CT quantification of in situ fabric evolution and shearing behaviour of granular soils of different particle shapes. *Can. Geotech. J.* **2024**, *61*, 2450–2467. [CrossRef]
20. Pereira, E.C.; Bell, C.A.; Urwin, P.E.; Tracy, S. The use of X-ray Computed Tomography revolutionises soil pathogen detection. *bioRxiv* **2024**. [CrossRef]
21. Ogilvie, C.M.; Ashiq, W.; Vasava, H.B.; Biswas, A. Quantifying Root-Soil Interactions in Cover Crop Systems: A Review. *Agriculture* **2021**, *11*, 218. [CrossRef]
22. Kan, X.; Zheng, W.; Cheng, J.; Zhangzhong, L.; Li, J.; Liu, B.; Zhang, X. Investigating Soil Pore Network Connectivity in Varied Vegetation Types Using X-ray Tomography. *Water* **2023**, *15*, 3823. [CrossRef]
23. Gaspareto, J.V.; Pires, L.F. X-ray Microtomography Analysis of Integrated Crop–Livestock Production's Impact on Soil Pore Architecture. *AgriEngineering* **2024**, *6*, 2249–2268. [CrossRef]
24. Chun, H.C.; Giménez, D.; Yoon, S.W. Morphology, lacunarity and entropy of intra-aggregate pores: Aggregate size and soil management effects. *Geoderma* **2008**, *146*, 83–93. [CrossRef]
25. San José Martínez, F.; Caniego, F.; García-Gutiérrez, C. Lacunarity of soil macropore space arrangement of CT images: Effect of soil management and depth. *Geoderma* **2017**, *287*, 80–89. [CrossRef]
26. de Oliveira, J.A.T.; Cássaro, F.A.M.; Posadas, A.N.D.; Pires, L.F. Soil Pore Network Complexity Changes Induced by Wetting and Drying Cycles—A Study Using X-ray Microtomography and 3D Multifractal Analyses. *Int. J. Environ. Res. Public Health* **2022**, *19*, 10582. [CrossRef]
27. Kravchenko, A.N.; Boast, C.W.; Bullock, D.G. Multifractal Analysis of Soil Spatial Variability. *Agron. J.* **1999**, *91*, 1033–1041. [CrossRef]
28. Soto-Gómez, D.; Pérez-Rodríguez, P.; Vázquez Juíz, L.; Paradelo, M.; López-Periago, J.E. 3D multifractal characterization of computed tomography images of soils under different tillage management: Linking multifractal parameters to physical properties. *Geoderma* **2020**, *363*, 114129. [CrossRef]
29. San José Martínez, F.; Martín, M.; Caniego, F.; Tuller, M.; Guber, A.; Pachepsky, Y.; García-Gutiérrez, C. Multifractal analysis of discretized X-ray CT images for the characterization of soil macropore structures. *Geoderma* **2010**, *156*, 32–42. [CrossRef]
30. Ju, X.; Jia, Y.; Li, T.; Gao, L.; Gan, M. Morphology and multifractal characteristics of soil pores and their functional implication. *CATENA* **2021**, *196*, 104822. [CrossRef]
31. Torre, I.; Losada, J.; Heck, R.; Tarquis, A. Multifractal analysis of 3D images of tillage soil. *Geoderma* **2018**, *311*, 167–174. [CrossRef]
32. Tarquis, A.; Heck, R.; Andina, D.; Alvarez, A.; Antón, J. Pore network complexity and thresholding of 3D soil images. *Ecol. Complex.* **2009**, *6*, 230–239. [CrossRef]
33. Soil Survey Staff. *Keys to Soil Taxonomy*, 13th ed.; U.S. Department of Agriculture, Natural Resources Conservation Service: Washington, DC, USA, 2022.
34. Teixeira, P.C.; Donagemma, G.K.; Fontana, A.; Teixeira, W.G. *Manual de Métodos de Análise de Solo*; Embrapa: Brasília, Brazil, 2017.
35. Dong, P. Lacunarity analysis of raster datasets and 1D, 2D, and 3D point patterns. *Comput. Geosci.* **2009**, *35*, 2100–2110. [CrossRef]
36. Lee, B.H.; Lee, S.K. Effects of specific surface area and porosity on cube counting fractal dimension, lacunarity, configurational entropy, and permeability of model porous networks: Random packing simulations and NMR micro-imaging study. *J. Hydrol.* **2013**, *496*, 122–141. [CrossRef]
37. Roy, A.; Perfect, E.; Dunne, W.M.; McKay, L.D. A technique for revealing scale-dependent patterns in fracture spacing data. *J. Geophys. Res. Solid Earth* **2014**, *119*, 5979–5986. [CrossRef]
38. The MathWorks, I. *MATLAB*, Version R2018a. 2018. Available online: https://www.mathworks.com (accessed on 5 October 2024).
39. Posadas, A.N.D.; Giménez, D.; Quiroz, R.; Protz, R. Multifractal Characterization of Soil Pore Systems. *Soil Sci. Soc. Am. J.* **2003**, *67*, 1361–1369. [CrossRef]

40. Posadas, A.N.D.; Quiroz, R.; Zorogastúa, P.E.; León-Velarde, C. Multifractal characterization of the spatial distribution of ulexite in a Bolivian salt flat. *Int. J. Remote. Sens.* **2005**, *26*, 615–627. [CrossRef]
41. Posadas, A.N.D.; Lourenço, A.L.F. *NASS: Non-Linear Analysis Scaling System*, Version II; Software Developed with the Support of the Department of Environmental Science; Rutgers, The State University of New Jersey: New Brunswick, NJ, USA, 2023.
42. Chun, H.C.; Gimenez, D.; Yoon, S.W.; Park, C.W.; Moon, Y.H.; Sonn, Y.K.; Hyun, B.K. Review of Soil Structure Quantification from Soil Images. *Korean J. Soil Sci. Fertil.* **2011**, *44*, 517–526. [CrossRef]
43. Klute, A.; Dirksen, C. Hydraulic conductivity and diffusivity: Laboratory methods. *Methods Soil Anal. Part 1 Phys. Mineral. Methods* **1986**, *5*, 687–734. [CrossRef]
44. van Genuchten, M.T. A Closed-form Equation for Predicting the Hydraulic Conductivity of Unsaturated Soils. *Soil Sci. Soc. Am. J.* **1980**, *44*, 892–898. [CrossRef]
45. Mualem, Y. A new model for predicting the hydraulic conductivity of unsaturated porous media. *Water Resour. Res.* **1976**, *12*, 513–522. [CrossRef]
46. Klute, A. Laboratory measurement of hydraulic conductivity of saturated soil. *Methods Soil Anal. Part 1 Phys. Mineral. Prop. Incl. Stat. Meas. Sampl.* **1965**, *9*, 210–221. [CrossRef]
47. Pessoa, T.N.; Libardi, P.L. Physical-hydric properties of Oxisols as influenced by soil structure and clay mineralogy. *CATENA* **2022**, *211*, 106009. [CrossRef]
48. Brewer, R. Fabric and mineral analysis of soils. *Soil Sci.* **1965**, *100*, 73. [CrossRef]
49. Santos, C.R.d.; Antonino, A.C.D.; Heck, R.J.; Lucena, L.R.R.d.; Oliveira, A.C.H.d.; Silva, A.S.A.d.; Stosic, B.; Menezes, R.S.C. 3D soil void space lacunarity as an index of degradation after land use change. *Acta Sci. Agron.* **2020**, *42*, e42491. [CrossRef]
50. Zeng, Y.; Payton, R.L.; Gantzer, C.J.; Anderson, S.H. Fractal Dimension and Lacunarity of Bulk Density Determined with X-ray Computed Tomography. *Soil Sci. Soc. Am. J.* **1996**, *60*, 1718–1724. [CrossRef]
51. Nunes, V.d.J.; Leite, E.d.S.; Maria de Lima, J.; Barbosa, R.S.; Santos, D.N.; Dias, F.P.M.; Nóbrega, J.C.A. Soil preparation systems and type of fertilization as affecting physical attributes of cohesive soil under eucalyptus in Northeastern Brazil. *Acta Sci. Agron.* **2022**, *45*, e58010. [CrossRef]
52. Vidal-Vázquez, E.; Camargo, O.; Vieira, S.; Miranda, J.; Menk, J.; Siqueira, G.; Mirás-Avalos, J.; Paz González, A. Multifractal Analysis of Soil Properties along Two Perpendicular Transects. *Vadose Zone J.* **2013**, *12*, 1–13. [CrossRef]
53. Yang, C.; Wu, J.; Li, P.; Wang, Y.; Yang, N. Evaluation of Soil-Water Characteristic Curves for Different Textural Soils Using Fractal Analysis. *Water* **2023**, *15*, 772. [CrossRef]
54. Chen, K.; Liang, F.; Wang, C. A fractal hydraulic model for water retention and hydraulic conductivity considering adsorption and capillarity. *J. Hydrol.* **2021**, *602*, 126763. [CrossRef]
55. Gao, Y.; Fu, Y.; Chen, J.; Sun, D. A novel equation for simulating the bimodal soil–water retention curve of unsaturated soils. *Acta Geotech.* **2024**, *19*, 5347–5362. [CrossRef]
56. Ribeiro, K.D.; Menezes, S.M.; Mesquita, M.d.G.B.d.F.; Sampaio, F.d.M.T. Propriedades físicas do solo, influenciadas pela distribuição de poros, de seis classes de solos da região de Lavras-MG. *Ciênc. Agrotec.* **2007**, *31*, 1167–1175. [CrossRef]
57. Bwambale, E.; Abagale, F.K.; Anornu, G.K. Smart irrigation monitoring and control strategies for improving water use efficiency in precision agriculture: A review. *Agric. Water Manag.* **2022**, *260*, 107324. [CrossRef]